Low-field giant magnetoresistance in (111)-textured Co/Au multilayers prepared with magnetron sputtering

S. Stavroyiannis, C. Christides,[a] and D. Niarchos
Institute of Materials Science, NCSR ''Demokritos,'' 153 10 Aghia Paraskevi, Attiki, Greece

Th. Kehagias, Ph. Komninou, and Th. Karakostas
Department of Physics, Aristotle University of Thessaloniki, 54006 Thessaloniki, Greece

(Received 30 January 1998; accepted for publication 2 September 1998)

A series of magnetron-sputtered $[\mathrm{Co}(1\ \mathrm{nm})/\mathrm{Au}(t_{\mathrm{Au}})]_{30}$ multilayers (MLs) has been deposited on Si(100) substrates covered with a 100 nm thick SiN_x buffer layer. The samples were examined with x-ray diffraction (XRD), magnetotransport (MR), isothermal magnetization (M-H), and transmission electron microscopy (TEM) measurements. The quality of the interface and layer stacking in these MLs was observed with cross-section TEM and examined with superlattice refinement of the XRD patterns, where an (111) preferred orientation is evident along the growth direction. Three MR maxima, with values $\Delta R/R_s = 3.5\%$, 1.3%, and 1.1% were observed for Au layer thicknesses (t_{Au}) of 2.5, 3.9, and 5.1 nm, respectively, in a range of applied magnetic fields less than ± 100 Oe, that are attributed to the giant magnetoresistance (GMR) effect. In the $[\mathrm{Co}(1\ \mathrm{nm})/\mathrm{Au}(2.4\ \mathrm{nm})]_{30}$ sample, the GMR coercivity is two orders of magnitude less than that observed in epitaxial structures. This makes the sputtered Co/Au MLs possible candidates for use in GMR applications. Below $t_{\mathrm{Au}} = 2$ nm a maximum anisotropic MR effect of 2% is observed for $t_{\mathrm{Au}} = 0.6$ nm. © *1998 American Institute of Physics.* [S0021-8979(98)05223-2]

I. INTRODUCTION

The giant magnetoresistance (GMR) effect occurs in a variety of magnetic systems including heterostructures and multilayers (MLs), spin valves, or granular materials.[1] In TM/NM MLs (TM=Fe, Co, Ni or $Ni_{81}Fe_{19}$ permalloy and NM=Cu, Ag, Au noble metals) the GMR ratio $MR_{max} = (R_{max}\text{-}R_s)/R_s$, with R_{max} the maximum and R_s the minimum resistance in different magnetic fields H, is an oscillating function of spacer thickness (t_{NM}) with maxima[1,2] corresponding to antiferromagnetic (AF) coupling between neighboring TM layers. Although the GMR effect is not of quantum origin[3] one has to apply a quantum-mechanical formalism, which explicitly takes into account the wave nature of electrons. This treatment leads to quantum size effects in the resistivity and magnetoresistance (MR) and gives rise to oscillations in: (i) the dependence of the resistivity of a single metallic film on the film thickness[4,5] and (ii) the GMR effect in magnetic sandwich structures.[3] It is commonly accepted that the GMR effect is due to spin-dependent scattering and both, experiments[6] and theoretical calculations[7] favor interface scattering as the most important mechanism. However, the question is still open[3,8] whether bulk scattering, originating from defects or impurities inside the magnetic and the spacer layers, or interface scattering dominates the GMR effect. Both can (in principle) cause a GMR effect and in combination they can even cancel each other provided that their spin asymmetry is opposite.[9]

In exchange-coupled MLs the models use extensions of the Ruderman–Kittel–Kasuya–Yosida (RKKY) oscillations through the spacer layer,[10] whose period depends on Fermi surface parameters, and spin-dependent potential wells[11] to explain theoretically the oscillatory GMR for polycrystalline Cu, and (001), (110)-oriented NM spacers.[12] However, in epitaxial or polycrystalline TM/NM MLs grown with a (111) preferred orientation[13–15] the observed oscillatory interlayer exchange coupling is markedly different from the theoretically predicted $1/t_{NM}$ (Ref. 2) dependence. Specifically, it has been argued[16] that in sputtered Fe/Cu/Fe and Co/Cu/Co MLs the minority grains with (100) preferred orientation may be responsible for the antiferromagnetic interlayer coupling, while the dominant (111)-textured grains account for their GMR. On the other hand, in Co/Cu(111) MLs grown by molecular beam epitaxy it is found[12] that the AF interlayer coupling at the first MR_{max} peak is of an intrinsic nature and is not due to a small amount of misaligned crystallites with (100) texturing. Thus, so far, it is not clear how the size of the GMR effect is related to the structural properties of the superlattice.

Co/Au(111) superlattices with perpendicular magnetic anisotropy were one of the structures in which the GMR effect was first reported.[17] After that, an antiparallel alignment of the magnetic moments between adjacent Co layers has been associated[18] with spin-dependent scattering and at a later date the oscillatory MR_{max} behavior has been assigned to oscillatory magnetic interactions, which were related[15] to the RKKY interlayer exchange coupling (AF). However, AF exchange coupling is not a necessary condition for the GMR to occur since the antiparallel alignment can be obtained also by other methods (Refs. 3 and 9, references therein). Thus, the major differences between the Co/Au(111) MLs and the other (111)-textured Co/NM MLs, that exhibit oscillatory GMR effect with t_{NM}, are:

[a]Electronic mail: christides@ims.ariadne-t.gr

(i) The Co layer stacking is usually hcp in Co/Au MLs[19] while in Co/Cu MLs,[20,21] it is fcc, and in Co/Ag MLs, it is a mixture of fcc, hcp, and stacking faults.[22]

(ii) The GMR Co/Au MLs exhibit perpendicular magnetic anisotropy[15,17] while in Co/Cu MLs the magnetic moments are always lying in the film plane. Generally, in Co/Au MLs the magnetic anisotropy is induced either by the magnetoelastic anisotropy, caused by the spin-orbit coupling[23] of hcp Co, which for $t_{Co}<2.3$ nm overcomes the in-plane shape anisotropy due to the spin–spin dipole interaction, or by the broken symmetry at the interfaces due to their sharpness.[24]

(iii) In Co/Au(111) MLs the large magnetocrystalline anisotropy[23] of hcp Co causes an alignment of the magnetic moments perpendicular to the film plane and creates a coercive field H_c of about 0.5 kOe in the GMR curves that precludes their use in GMR applications.

Practical applications of GMR sensors require large GMR ratios and zero hysteresis in the GMR curves. Thus, in the case of Co/Au MLs modification of Co layering from hcp to fcc stacking is expected to reduce the magnetocrystalline anisotropy and the H_c. Traditionally, sputtering has represented a comparatively simple and rapid method for preparing thin films with a large variety of microstructural features that are adjusted by the deposition conditions to fit their extrinsic properties for applications. In recent years, there has been great activity and interest in the Co/Cu system, grown with (111) texturing, because it exhibits the largest GMR ratios and oscillatory interlayer exchange coupling for sputtered MLs. Early studies on GMR MLs[1,2] have shown that spacer layers comprising the nonferromagnetic $3d$, $4d$, and $5d$ metals exhibit a decrease of the interlayer exchange coupling strength down each column in the periodic table. Since noble metal spacer layers give some of the largest GMR values, it is shown[25] that high aspect ratios for low external fields can be achieved for magnetic MLs comprising Au spacer layers.

To the best of our knowledge, the only system of *sputtered* TM/Au MLs that exhibits oscillatory MR with a period of $t_{Au}\approx 1.2$ nm, is reported for untextured $Ni_{81}Fe_{19}$/Au films,[25] while the most recent results for Co/Au-sputtered MLs[26] show interesting magneto-optical properties. In the present study, as-prepared Co/Au MLs grown by magnetron sputtering exhibit a GMR oscillation with t_{Au}, and a useful change in GMR ratio per unit field for the $[\mathrm{Co}(1\,\mathrm{nm})/\mathrm{Au}(2.5\,\mathrm{nm})]_{30}$ composition.

II. EXPERIMENTAL DETAILS

A series of $[\mathrm{Co}(1\,\mathrm{nm})/\mathrm{Au}(t_{Au})]_{30}$ MLs was grown on top of Si(100) substrates with a 100 nm thick SiN_x buffer layer. Metallic disks of 99.99% pure elements with a diameter of 5 cm, were used as target materials in a high vacuum Edwards E360A sputtering system with a cluster of ATOM-TECH 320-SE planar magnetron sputter sources. The substrates were cut before deposition in dimensions of $12\times 4\,\mathrm{mm}^2$. During deposition the $Si(100)/SiN_x$ substrates were thermally isolated from the water-cooled supporting table. All samples were deposited in a cryogenically pumped chamber with a base pressure of 6×10^{-7} Torr under an Ar (99.999% pure) pressure of 3 mTorr. A rf magnetron gun operating at 30 W with a deposition rate of 0.09 nm/s was used for Co, and dc sputtering at 5 W for Au, resulting in a rate of 0.12 nm/s. Determination of the thickness of the various layers was based on the deposition time assuming constant deposition rates. The bilayer thickness has been measured with low-angle x-ray diffraction (XRD) profiles and confirmed by cross-section transmission electron microscopy (XTEM). XRD spectra were collected with a SIEMENS D500 powder diffractometer in θ–2θ scans, using Cu $K\alpha$ radiation. TEM observations were carried out in a Jeol JEM 120 CX electron microscope operated at 120 kV. XTEM specimens were prepared using the standard techniques of mechanical thinning combined with appropriate ion milling.

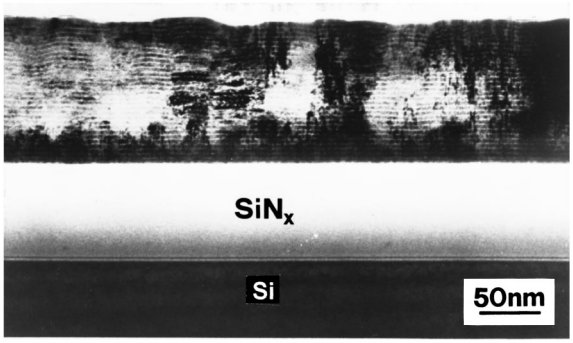

FIG. 1. Bright-field (BF) image illustrating the structural profile of the system. The Co/Au layers are depicted, over the SiN_x buffer layer, as bright and dark bands, respectively.

Magnetic hysteresis loops were measured with a Quantum Design MPMSR2 superconducting quantum interference device (SQUID) magnetometer. MR measurements were performed at 300 K with the four-point-probe method, using a dc current of 1 mA. The field H was applied in three directions relative to the film plane and the current direction: one with H lying in the film plane vertical to the current direction (transverse), the second with H lying in the film plane parallel to the current (longitudinal), and the third with H perpendicular to the film. All measurements were performed at 300 K by first applying the maximum positive field H parallel to the film plane and then completing the loop.

III. EXPERIMENTAL RESULTS

A. TEM observations

TEM measurements concern the $[\mathrm{Co}(1\,\mathrm{nm})/\mathrm{Au}(2.5\,\mathrm{nm})]_{30}$ film with maximum GMR. The architecture of the system is illustrated in the bright-field (BF) image of Fig. 1. The lower layer is the Si substrate oriented with the [110] zone axis parallel to the electron beam. Over the amorphous SiN_x buffer layer the Co/Au layers are imaged as successive bright and dark bands, respectively. In Fig. 1 it is evident that the interfacial roughness of the Co/Au layers increases as the distance from the buffer layer increases. In order to estimate the interlayer thickness and sharpness, a magnified area of the multilayer is depicted in Fig. 2(a). It is

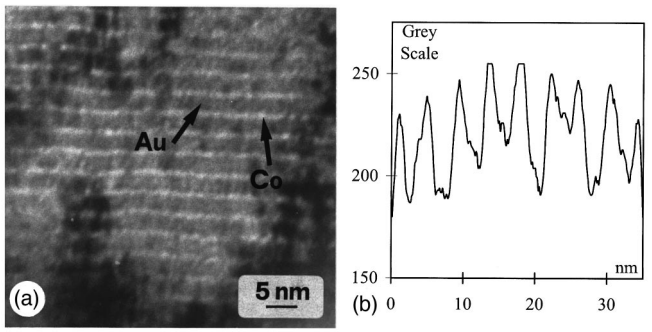

FIG. 2. (a) A high magnification image of a multilayer area showing the morphology of the Co/Au interlayer. The Au layers appear thicker due to interdiffusion at the interfaces. (b) A line profile showing the contrast variation across a series of nine successive bilayers.

deduced that the thickness of the Co/Au bilayers remains rather constant at 3.5 ± 0.05 nm for all repetitions. Figure 2(b) shows a line profile of the contrast intensity across the layers, which is not of a rectangular shape and indicates the existence of interfacial disorder.

Figure 3 shows a diffraction pattern from an area of Fig. 1. It contains reflections from the multilayer and the Si substrate. The reflections of Si were used as an internal calibration for the precise determination of the crystallographic parameters of the multilayer structure. The diffraction from the multilayer contains reflections of the [110] zone axis of Au, with the 111 reflection parallel to the 004 reflection of Si. This indicates that the (111) planes of Au are oriented parallel to the (001) planes of Si. Since in similarly prepared Co/Cu multilayers the (111) Cu planes also exhibit[27] a preferential orientation parallel to the (001) planes of Si, it is evident that the 100 nm SiN_x buffer layer transfers the imposed orientation from the Si(100) substrate texture and provides a flat surface, in atomic scale, for deposition. In addition, all reflection spots are elongated and show that the multilayer is composed of small adjacent misoriented crystallites. Crystallographic analysis of the diffraction pattern shows that the d spacing of the (111) planes is $d_{111} = 0.229 \pm 0.001$ nm, in agreement with the averaged, over all Co and Au layers, out-of-plane lattice parameter observed from the XRD data.

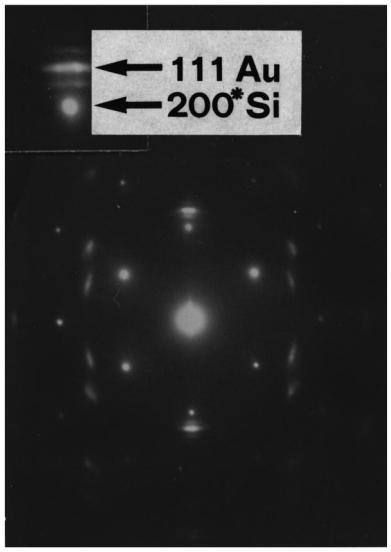

FIG. 3. A diffraction pattern containing reflections from the MLs and the Si substrate. The elongated reflections belong to the MLs. A magnified part of the diffraction, illustrating the satellites arising from the modulation, is given as an inset. The 2 0 0* forbidden reflection of Si appears from double diffraction.

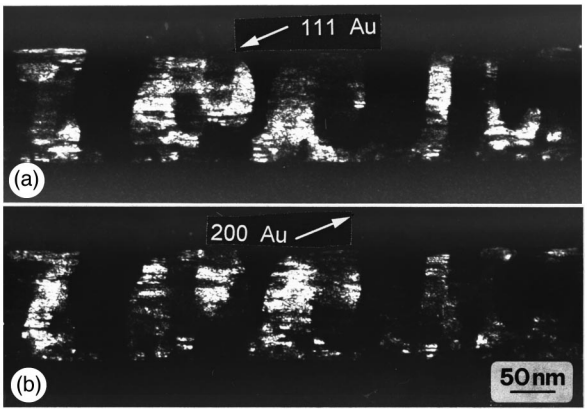

FIG. 4. Dark-field (DF) images of the MLs showing the columnar mode of growth and the existence of (111) growth twins. (a) $g = 1\bar{1}1$ reflection of Au. (b) $g = 2\ 0\ 0$ reflection of Au from twinned crystals.

The diffraction pattern in Fig. 3 is a composite pattern containing additional reflections arising from twin crystals that have as twin planes the (111) plane of growth. The modulation is also verified from the existence of satellite reflections, which are shown in a magnified part of the diffraction pattern, given as an inset in Fig. 3. Figure 4(a) is a dark-field (DF) image, taken with the $1\bar{1}1$ reflection of Au, that reveals a characteristic columnar mode of growth. In addition, the observed surface roughness in Fig. 1 is a representative feature resulting from columnar growth in strained multilayer structures.[28] Figure 4(b) is another DF image from the same area taken with a 2 0 0 twinning reflection. Both DF images show that the twins are formed into the same column. Since the columns grow throughout the MLs or they are extended over many successive layers, their crystal structure should be homogeneous. This leads to the conclusion that an average fcc-modulated lattice is formed in every columnar structure of the MLs. Such a conclusion is also supported by the existence of numerous {111} twins that appear in the columns. Therefore, throughout a column, Co and Au form successive layers that grow epitaxially. Thus, Co should be of a cubic nature, although no characteristic Co reflections were detected in the diffraction patterns.

B. XRD spectra and SUPREX analysis

Representative XRD profiles at the low- (top), medium- (middle), and high- (bottom) angle regions are shown in Fig. 5 for the $[\mathrm{Co}(1\ \mathrm{nm})/\mathrm{Au}(2.5\ \mathrm{nm})]_{30}$ film, where the highest GMR ratio is observed. The observation of four well-defined superlattice Bragg peaks at low-angle spectra indicates[24] the existence of sharp Co/Au interfaces. In the medium and high-angle regions satellite peaks with asymmetric intensities were observed below and above the zero-order reflec-

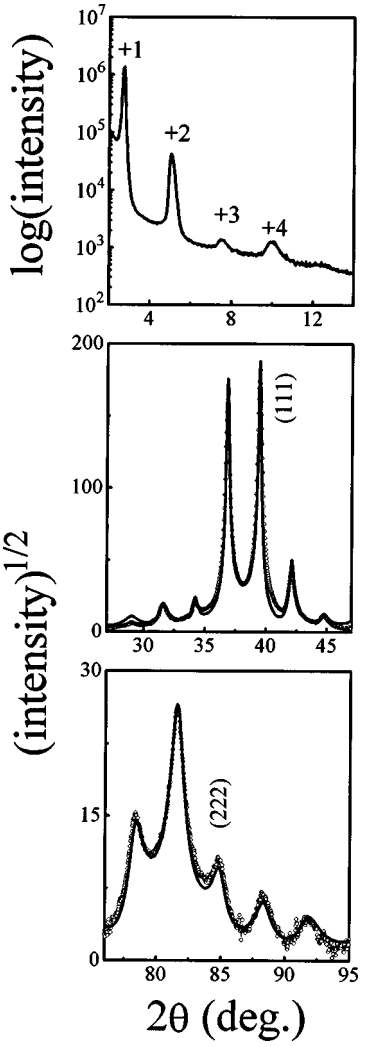

FIG. 5. The XRD profiles are shown at low-, medium-, and high-angle regions for the $[Co(1\ nm)/Au(2.5\ nm)]_{30}$ film where the maximum GMR ratio is observed. The solid line corresponds to the best fit obtained by SUPREX analysis.

tions at $2\theta = 39.463°$ ($d_{111} = 0.2282$ nm) and $2\theta = 84.782°$ ($d_{222} = 0.1143$ nm) positions, that are indexed into (111) and (222) fcc Bragg peaks, respectively. Comparatively, the corresponding bulk value for fcc Au is $d_{111}(Au) = 0.2355$ nm, for hcp Co in the [0001] direction it is $d_{0002}(Co) = 0.2023$ nm, while for fcc Co it is $d_{111}(Co) = 0.2047$ nm and $d_{222}(Co) = 0.1023$ nm. When the Co layers are coherent with the Au layers, they are under tensile stress because the atomic size difference between Co and Au is as large as 15%. Thus, the lattice mismatch between fcc Au and hcp Co is 0.0332 nm in the (111) direction of Au and slightly smaller for fcc Co (0.0308 nm).

In order to obtain information on the stacking of atomic planes in the (111) direction of Au, the observed spectra were fitted by using the superlattice refinement (SUPREX) program[29] developed to allow a quantitative comparison between the model calculations and the measured profiles. Since our low-angle observed profiles are not reliable for quantitative analysis only the medium- (MAS) and high-angle satellite (HAS) peaks are used. For convenience, the

TABLE I. The obtained parameters from the SUPREX refiniment of the $[Co(1\ nm)/Au(2.5\ nm)]_{30}$ film, where the maximum GMR ratio is observed.

Parameter	Co	Au
d spacing (nm)	0.2098	0.237
Number of atomic planes/layer N	5.2	10.4
s_{Co} and s_{Au} (in atomic planes)	0.2	0.7
Total layer thickness $t = N \times d$ (nm)	1.09	2.27
''Bulk'' layer thickness t_b (nm)	0.878	2.235
Interface layer thickness $t_i = t\text{-}t_b$ (nm)	0.213	0.237
Interface layer contraction Δd_1 (nm)	−0.022	−0.006
Interface layer expansion Δd_2 (nm)	0.018	0.011

MAS peak positions are usually indexed about the average lattice constant $\bar{d}$:

$$\frac{2 \sin \vartheta}{\lambda_x} = \frac{1}{\bar{d}} \pm \frac{n}{\Lambda}, \tag{1}$$

where n is an integer that labels the order of the satellite around the main Bragg peak, λ_x the wavelength of x rays, $\Lambda = t_{Co} + t_{Au} + t'$ (t' = total interface thickness), and $\bar{d} = \Lambda/(N_A + N_B)$, with N_A, N_B the number of atomic planes of material A and B in one bilayer. From the peak positions $\bar{d}$ and Λ can be determined directly. According to Ref. 30, the crystalline layer is described by N atomic planes, which are separated by a lattice constant d. The distribution of the number of planes N_j for Co and Au layers is given by a discrete distribution about the mean values N_{Co} and N_{Au} with widths s_{Co} and s_{Au}. For every layer three atomic planes near the interface are allowed to expand or contract an amount $\Delta d_1 e^{-n\alpha}$ and $\Delta d_2 e^{-n\alpha}$ on the bottom and top, respectively, where $n = 0,1,2$ corresponds to atomic planes away from the interface. These parameters account for the interface thickness or roughness t_i in the average layer thickness: $t_A = N_A \times d_A = t_b + t_i$, where t_b is the ''bulk'' layer thickness of the relaxed lattice.

The interlayer disorder is also taken into account in the SUPREX fitting procedure. Interlayer disorder refers to deviations in the periodicity of the layers along the growth direction that result from layer thickness variations and interface disorder. The parameters of interface distance h and interface fluctuation width c are related to the degree of interface (interlayer) disorder. For a lattice-mismatched incoherent interface, the interface distance h (structural roughness) varies in a continuous manner, described with a Gaussian distribution, and the interface fluctuation c (disorder) is the width of the Gaussian.

The best fit, achieved with exactly the same structural parameters in MAS and HAS patterns, is shown with the solid line in Fig. 1 for the $[Co(1\ nm)/Au(2.5\ nm)]_{30}$ film and the obtained parameters are listed in Table I. The estimated $\Lambda = 3.563$ nm and the t_b values from Table I indicate that there is a rough bilayer interface $t' = 0.45$ nm. This corresponds to two atomic planes at the interface of Co/Au and is a measure of their sharpness. The obtained interface distance $h = 0.226$ nm, with an interface fluctuation (disorder) width $c = 0.013$ nm, gives an estimation of the lattice mismatch

that is almost equal to the average separation distance: $(d_{Au}+d_{Co})/2$ of Co and Au atomic planes. The SUPREX fitting reveals information for two important structural features:

(i) ''Bulk'' t_{Co} and t_{Au} values correspond to four and nine atomic planes per layer, respectively, while the t_i values in Table I are about one atomic plane of Co and Au thick. If a layer-by-layer growth mode is assumed, then the in-plane Co layers will be expanded and Au layers will be in-plane compressed, as in Co/Cu(111) superlattices.[31] Such in-plane Co expansion together with the out-of-plane d_{Co}-spacing expansion (Fig. 5) will result in a three-dimensional volume expansion of the unit cell that is not favored from the increase of lattice strain energy. Spin echo ^{59}Co nuclear magnetic resonance (NMR) spectra in these Co/Au MLs have revealed[32] a significant modification in Co atomic packing that is different from the hcp or the fcc stacking. In the fitting model the NMR spectra were reconciled with a high concentration (~12%) of Co vacancies. Therefore, it is reasonable to assume that, kinetically grown, prismatic dislocations are formed in the atomic planes of Co. These kinds of structural modifications are expected to control the micromagnetic structure within the Co layers.

(ii) In Table I the d_{Co} and d_{Au} spacings are both larger than their bulk values by 2.5% for fcc Co, 3.7% for hcp Co, and 0.6% for Au. Since the obtained d_{Co} spacing expansion is less than the 15% expected from the Co/Au(111) lattice mismatch, and the estimated interface roughness is limited to two atomic planes of Co–Au, this suggests that the Co/Au interfaces are incoherent.

Considering incoherent interfaces, the variation of d_{111} $(=\overline{d})$ interatomic spacings as a function of the fractional Au thickness $p=t_{Au}/\Lambda$ is plotted in Fig. 6 (bottom). These d_{111} values were determined from the position of the fundamental (111) Bragg peak and they express an out-of-plane lattice parameter averaged over all Co and Au layers. A linear fit (solid line) of these data gives a $d_{111}(\mathrm{Au})=0.2355$ nm for $p=100\%$ (pure fcc Au) and a $d_{111}(\mathrm{Co})=0.2096$ nm for $p=0\%$ (pure Co). These values are in agreement with the bulk d spacing of Au and the estimated d_{Co} value in Table I for the $[\mathrm{Co}(1\ \mathrm{nm})/\mathrm{Au}(2.5\ \mathrm{nm})]_{30}$ film.

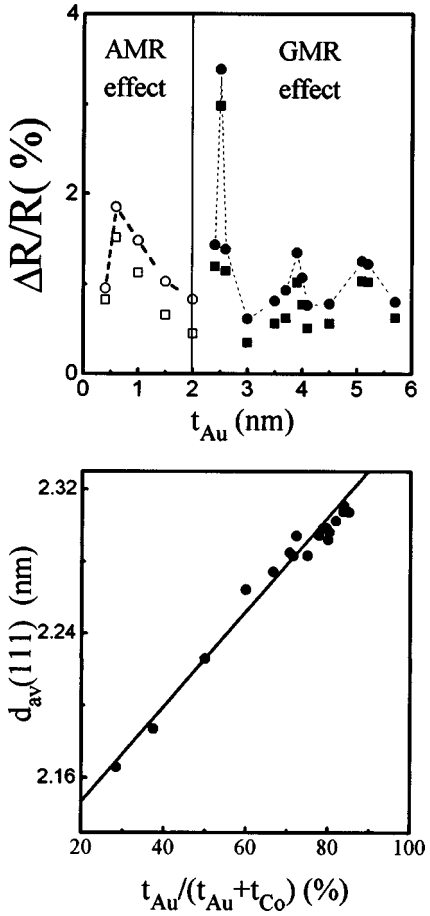

FIG. 6. Variation of the MR ratio $[R_{max}\text{-}R(H_s)]/R(H_s)$ as a function of t_{Au}, with H applied in the film plane vertically (circles) and parallel (squares) to the current flow direction. The variation of the $d_{111}(=\overline{d})$ spacings, determined from the position of the fundamental Bragg peak, is plotted against the fractional Au thickness: $p=t_{Au}/\Lambda$.

C. Magnetization and magnetoresistance measurements

In Fig. 6 (top) is shown the variation of the MR ratio $[R_{max}-R(H_s)]/R(H_s)$, where H_s is the saturation field, as a function of t_{Au} with H applied in the film plane vertical (circles, $R_\perp$) and parallel (squares, $R_\parallel$) to the current flow direction. A characteristic change has been observed in the shape of the MR(H) curves above and below $t_{Au}\approx 2.3$ nm. For $t_{Au}>2.3$ nm, three well-defined MR maxima, with values $\Delta R/R=3.5\%\pm0.1\%$, $1.3\%\pm0.1\%$, and $1.1\%\pm0.1\%$ were observed for Au layer thicknesses (t_{Au}) of 2.5, 3.9, and 5.1 nm (~10, 16, and 22 Au atomic planes), respectively, in a range of applied magnetic fields less than ± 60 Oe, and were attributed to the GMR effect. A residual MR ratio of 0.3%–0.5% appears in t_{Au} regions where the interlayer coupling is expected to be ferromagnetic. This effect is usually observed in polycrystalline GMR multilayers[1] and can be attributed to intralayer (bulk) spin-dependent scattering or to interfacial scattering from a small fraction of grains that exhibit antiparallel alignment among adjacent layers due to statistical deviations in spacer layer thickness (interface roughness). The period of the MR oscillations is different from that observed in epitaxial grown Co/Au(111)/Co trilayers[15] where the MR maxima occur for $t_{Au}\approx 5$, 9 and 14 atomic planes (1.2, 2.1, and 3.3 nm). Epitaxial trilayers exhibit a mean oscillation period of 4.5 atomic planes, in agreement with the theoretical prediction of 4.83 atomic planes[10] for oscillating coupling through Au(111). Comparing the t_{Au} values at the GMR maxima is evident that our first GMR peak (~10 atomic planes of Au) is near the second GMR maximum of the trilayer in Ref. 15. This indicates that for $t_{Au}=2.5$ nm the GMR effect is mainly due to interfacial spin-dependent scattering. The longitudinal Kerr-effect hysteresis loop has revealed[33] a manifold loop with insignificant residual magnetization for $t_{Au}=2.5$ nm, inferring coexistence of the so-called[34,35] ''bilinear'' and ''biquadratic'' interlayer coupling terms at this GMR maximum. However, in the second GMR maximum ($t_{Au}=3.9$ nm) there is a ferromagnetic Kerr-effect loop, that is characteristic of a random distribution of Co magnetic moments, resulting from mag-

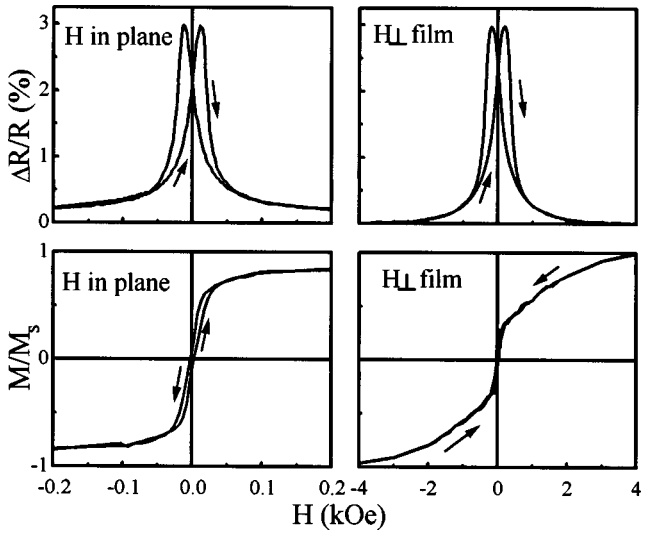

FIG. 7. Isothermal loops of the reduced magnetization M/M_s with H applied parallel to the long axis (on the left) and perpendicular (on the right) to the film plane. The transverse field ($H\perp I$) GMR loop, with H lying in the film plane (on the left), and the GMR loop for H perpendicular to film plane (on the right) are shown. All measurements concern the $[\mathrm{Co}(1\ \mathrm{nm})/\mathrm{Au}(2.5\ \mathrm{nm})]_{30}$ film.

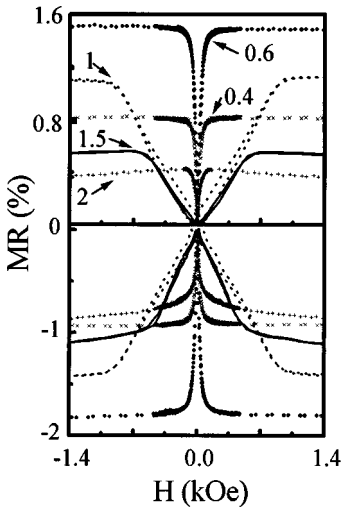

FIG. 8. The observed AMR curves are shown for (bottom) the transverse ($I\perp H$) and (top) longitudinal ($I\|H$) field configuration. The Au layer thickness values are indicated for $t_{\mathrm{Au}}=0.4$ nm ($\times$), 0.6 nm (circles), 1 nm (short dash), 1.5 nm (solid line), and 2 nm ($+$).

netically uncoupled layers. Thus, we may conclude that above $t_{\mathrm{Au}}=2.5$ nm the magnetic coupling between adjacent Co layers is decreasing and the GMR effect is reduced because the spin-dependent scattering occurs[9] from a smaller number of neighboring Co regions with antiparallel alignment of magnetic moments. Surprisingly, the oscillatory period of 6 atomic Au planes in our Co/Au(111) MLs is the same with that observed in Co/Cu(111) MLs[1,13] where the Co layer stacking is fcc.

For the $[\mathrm{Co}(1\ \mathrm{nm})/\mathrm{Au}(2.5\ \mathrm{nm})]_{30}$ sample we show in Fig. 7: at the bottom, the reduced magnetization M/M_s isothermal loop with H applied in plane (on the left) and perpendicular (on the right) to film plane; on top the transverse field ($H\perp I$) GMR loop with H lying in the film plane (on the left) and the GMR loop with H perpendicular (on the right) to the film plane. A comparison of the magnetic loop shapes and the large differences of H_s values, observed in the GMR loops, indicates that the magnetization is lying in the film plane. The in-plane M/M_s versus H loop has the typical shape of an antiferromagnetic material, implying that the magnetic moments between adjacent Co layers are AF coupled. In addition, for the transverse field GMR loop the drop in resistance is saturated at $H_s\approx 30$ Oe and leads to changes in resistance per unit field (efficiency) of about 0.11%/Oe at room temperature (RT). This efficiency is an order of magnitude less than the 4%/Oe observed[36] in anisotropic magnetoresistance (AMR) films of $Ni_{81}Fe_{19}$ and the 1%/Oe observed in GMR $Ni_{81}Fe_{19}$/Au MLs.[25] For the field applied perpendicular to the film plane an $H_s\approx 560$ Oe is observed that gives an efficiency of about 0.006%/Oe. For $t_{\mathrm{Au}}<2.3$ nm the longitudinal ($R_{\|}$) and transverse ($R_{\perp}$) MR curves are ascending and descending, respectively, by increasing the magnetic field (Fig. 8). The observed curves are typical of the AMR effect, arising from the ferromagnetic arrangement of adjacent magnetic moments[36] in the MLs. Note that the displayed values are not calculated with the usual formula for the AMR ratio$=(R_{\|}-R_{\perp})/(R_{\|}+R_{\perp})$, in order to be comparable with the GMR ratios for $t_{\mathrm{Au}}>2.3$ nm. The anisotropic MR variation with t_{Au} exhibits a similar behavior to that observed in $[\mathrm{Co}(0.3\ \mathrm{nm})/\mathrm{Au}(t_{\mathrm{Au}}]_{40}$ MLs,[37] grown on glass substrates by electron-beam evaporation, where a maximum AMR ratio appears for $t_{\mathrm{Au}}\approx 0.6$ nm in both cases. Figure 8 (bottom) shows the observed AMR curves for the transverse ($I\perp H$) and Fig. 8 (top) shows the longitudinal ($I\|H$) configuration. Remarkably, a considerable change in the shape of the MR curve is observed for $t_{\mathrm{Au}}=1.5$ and 1.0 nm, which fall in the Au thickness range where a perpendicular anisotropy is reported.[37–39] For $t_{\mathrm{Au}}<1$ nm the strength of the magnetocrystalline anisotropy is reduced and as a result AMR curves with low saturation fields are observed again.

Figure 9 shows the variation of the coercive field H_c (top) and the saturation field H_s (bottom) values, deduced from the AMR and GMR curves with transverse in-plane field geometry, as a function of t_{Au}. At first, it is obvious that the AMR ratios (Fig. 2, top) do not follow the variation of the corresponding H_c and H_s parameters for $t_{\mathrm{Au}}\leqslant 2$ nm, while for $t_{\mathrm{Au}}>2$ nm the GMR ratios follow the variation of H_s and provide evidence for interlayer exchange coupling among the Co layers. Second, there is an order of magnitude change in the H_c and H_s peak values between the t_{Au} regions where either the AMR or the GMR effect is predominant. These two features indicate that:

(i) for $t_{\mathrm{Au}}\leqslant 2$ nm the Co layer magnetic anisotropy ($\propto H_c$) determines the rotation of magnetic moments ($\propto H_s$) in the film plane; and

(ii) for $t_{\mathrm{Au}}>2$ nm the $H_s(\sim 15-30$ Oe) and H_c (~ 10 Oe) values are similar to those observed in TM/NM MLs, where the interlayer exchange coupling strength via the NM spacer layer determines the GMR properties[1,25] while the contribution from the magnetic layer anisotropy is insignificant. The small H_c values indicate that the Co layer an-

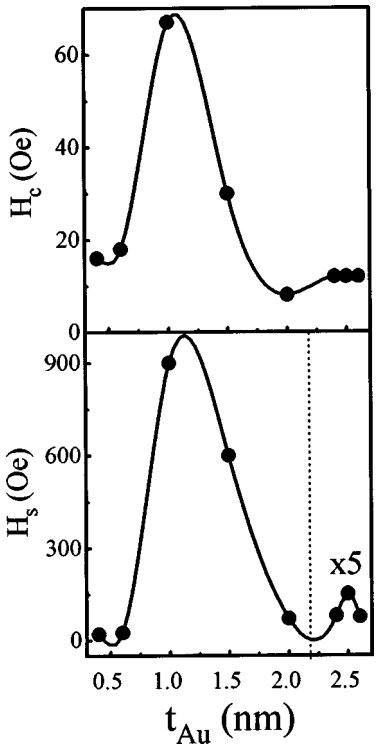

FIG. 9. Variation of the coercive field H_c and the saturation field H_s values, deduced from the AMR and GMR curves with transverse in-plane field geometry, as a function of the Au layer thickness t_{Au}.

isotropy is rather isotropic (cubic) and not uniaxial, as in structures with hexagonal or tetragonal symmetry. In addition, the H_s values are much smaller relative to those observed in Co/Cu and Co/Ag MLs.[1] This is in agreement with the observation that for $3d$, $4d$, and $5d$ noble metals the interlayer exchange coupling strength decreases down each column in the periodic table.[1,6,25] Thus, contrary to results reported earlier for this system,[6,15] our results show that in sputtered Co/Au(111) MLs it is possible to achieve low in-plane switching fields and GMR curves with very small hysteresis.

IV. DISCUSSION AND CONCLUSIONS

In brief, our sputtered MLs present the following differences from the epitaxial trilayers:[15]

(i) The GMR maximum for $t_{Au} \approx 1$ nm, corresponding to the first AF peak in exchange-coupled superlattices, is not achieved. Instead, only an AMR effect was observed for $t_{Au} < 2$ nm.

(ii) For $t_{Au} > 2$ nm the obtained GMR maxima occur with a mean oscillation period of 6 atomic Au planes, as in Co/Cu(111) multilayers.

(iii) For $t_{Au} = 2.5$ nm the coercive field H_c, where the GMR maximum value is observed, and the switching field H_s, where the GMR ratio approaches its lower value from both sides around H_c, are 0.01 and ± 0.03 kOe, respectively. Furthermore, in our multilayers the magnetization is lying in the film plane whereas in epitaxial trilayers[15] the perpendicular anisotropy term is dominant. In comparison, the observed values from the trilayers[9,15] are $H_c \approx 0.5$ kOe and $H_s \approx \pm 0.05$ kOe. This order of magnitude improvement of H_c indicates that sputter grown Co/Au MLs can be considered as possible candidates for use in GMR applications.

(iv) The maximum obtained GMR ratio of 3.1% is about 1% higher than that observed in epitaxial trilayers.

The observed differences between epitaxial trilayers or multilayers and our sputtered films may be attributed to structural modifications in the stacking of the Co layers. *Kinetically* grown nanostructures of Co can be obtained when the growth of the absorbate Co layer is determined by heterogeneous nucleation at intrinsic defects on the underlying Au layer or the substrate. These defects can be steps on a vicinal surface[40] or particular sites on a reconstructed surface.[41] It has been observed[19] that at the close-packed (111) surface of Au layers there are reconstructed domains separated with two kinds of boundaries: step edges and kink positions. Thus, it is found[19] that during deposition of Co on Au(111), a hcp stacking is favored only when large Co islands nucleate at the kink sites. Since in our case the Co layer stacking is not hcp, it can be argued that the used deposition conditions alter the Co coverage during growth of Co on Au(111) surfaces by changing the size of Co islands nucleating at the Au step edges (fcc stacking) relative to those formed at kink sites (hcp stacking).

In summary, it is shown that magnetron-sputtered Co/Au MLs with (111) texturing exhibit a low-field GMR effect, for $t_{Au} > 2$ nm, with small coercive and switching fields. Deposition of Co/Au MLs on SiN_x buffer layers seems to enable the development of a considerable fraction of faults in the stacking of Co along the growth direction. Indeed, spin echo ^{59}Co nuclear magnetic resonance spectra,[26] from the same Co/Au films, exhibit a unique profile that cannot be assigned to any of the known crystalline or glassy Co structures. Thus, the observed differences in magnetotransport properties, among the here examined Co/Au MLs and those reported by now, are attributed to the development of a specific microstructure in the magnetic layers. The $[\mathrm{Co}(1\,\mathrm{nm})/\mathrm{Au}(2.5\,\mathrm{nm})]_{30}$ film exhibits a GMR ratio of 3.5% at RT with $H_s \approx 30$ Oe, leading to changes in resistance per unit field (efficiency) of about 0.11%/Oe.

ACKNOWLEDGMENTS

This work has been supported by the EKBAN-280 project of the General Secretariat for Research and Technology of the Development Ministry in Greece. The SUPREX refinement program was developed with funds provided by the U.S. Department of Energy and the Belgian Interuniversity Attraction Pole Program.

[1] *Ultrathin Magnetic Structures II*, edited by B. Heinrich and J. A. C. Bland (Springer, Berlin, 1994), Chap. 2.
[2] S. S. P. Parkin, Phys. Rev. Lett. **67**, 3598 (1991).
[3] J. Barnas and Y. Bruynseraede, Phys. Rev. B **53**, 5449 (1996).
[4] M. Jalochowski and E. Bauer, Phys. Rev. B **37**, 8622 (1988).
[5] D. Calecki, Phys. Rev. B **43**, 11581 (1991).
[6] S. S. P. Parkin, Phys. Rev. Lett. **71**, 1641 (1993).
[7] K. M. Schep and G. E. W. Bauer, Phys. Rev. Lett. **78**, 3015 (1997).
[8] P. Zahn, J. Binder, I. Mertig, R. Zeller, and P. H. Dederichs, Phys. Rev. Lett. **80**, 4309 (1998).
[9] R. Shad, P. Belien, G. Verbanck, C. D. Potter, H. Fischer, S. Lefebvre, M.

Bessiere, V. V. Moshchalkov, and Y. Bruynseraede, Phys. Rev. B **57**, 13692 (1998).
[10] P. Bruno and C. Chappert, Phys. Rev. Lett. **67**, 1602 (1991); Phys. Rev. B **46**, 261 (1992).
[11] D. M. Edwards, J. Mathon, R. B. Muniz, and M. S. Phan, Phys. Rev. Lett. **67**, 493 (1991); J. Phys.: Condens. Matter **3**, 4941 (1991).
[12] R. Coehoorn, M. T. Johnson, W. Folkerts, S. T. Purcell, N. W. E. McGee, A. De Veirman, and P. J. H. Bloemen, NATO ASI Ser., Ser. B **309**, 295 (1993).
[13] S. S. P. Parkin, R. Bhadra, and K. P. Roche, Phys. Rev. Lett. **66**, 2152 (1991).
[14] S. S. P. Parkin, R. F. C. Farrow, R. F. Marks, A. Cebollada, G. R. Harp and R. J. Savoy, Phys. Rev. Lett. **72**, 3718 (1994).
[15] V. Grolier, D. Renard, B. Bartelian, P. Beauvillain, C. Chappert, C. Dupas, J. Ferre, M. Galtier, E. Kolb, M. Mulloy, J. P. Renard, and P. Veilet, Phys. Rev. Lett. **71**, 3023 (1993).
[16] W. F. Egelhoff, Jr. and M. T. Kief, Phys. Rev. B **45**, 7795 (1992).
[17] E. Velu, C. Dupas, D. Renard, J. D. Renard, and J. Seiden, Phys. Rev. B **37**, 668 (1988).
[18] C. Dupas, P. Beauvillain, C. Chappert, J. P. Renard, F. Tigui, P. Veillet, E. Velu, and D. Renard, J. Appl. Phys. **67**, 5680 (1990).
[19] B. Voigtlander, G. Meyer, and N. M. Amer, Phys. Rev. B **44**, 10354 (1991).
[20] J. de la Figuera, J. E. Prieto, C. Ocal, and R. Miranda, Phys. Rev. B **47**, 13043 (1993).
[21] T. J. Minvielle, R. J. Wilson, and R. L. White, Appl. Phys. Lett. **68**, 15027 (1996).
[22] E. A. M. van Alphen and W. J. M. de Jonge, Phys. Rev. B **51**, 8182 (1995).
[23] D. Weller, J. Stohr, R. Nakajima, A. Curl, M. G. Samant, C. Chappert, R. Megy, P. Beauvillain, P. Veillet, and G. A. Held, Phys. Rev. Lett. **75**, 3752 (1995).
[24] F. J. A. den Broeder, D. Kuiper, A. P. van de Mosselaer, and W. Hoving, Phys. Rev. Lett. **60**, 2769 (1988).
[25] S. S. P. Parkin and T. Rabedeau, Appl. Phys. Lett. **68**, 1162 (1996).
[26] Y. Liu, Z. S. Shan, and D. J. Sellmeyer, J. Appl. Phys. **81**, 5061 (1997).
[27] C. Christides, S. Stavroyiannis, N. Boukos, A. Travlos, and D. Niarchos, J. Appl. Phys. **83**, 3724 (1998).
[28] N. K. Flevaris and Th. Karakostas, J. Appl. Phys. **63**, 1228 (1988).
[29] I. K. Schuller, Phys. Rev. Lett. **44**, 1597 (1980); W. Sevenhans, M. G. Gijs, Y. Bruynseraede, H. Homma, and I. K. Schuller, Phys. Rev. B **34**, 5955 (1986).
[30] E. E. Fullerton, I. K. Schuller, H. Vanderstraeten, and Y. Bruynseraede, Phys. Rev. B **45**, 9292 (1992).
[31] P. Bodeker, A. Abromeit, K. Brohl, P. Sonntag, N. Metoki, and H. Zabel, Phys. Rev. B **47**, 2353 (1993).
[32] C. Christides, S. Stavroyiannis, M. Wojcik, S. Nadolski, E. Jedryka, and D. Niarchos, Phys. Rev. B (to be published).
[33] C. Christides, R. Lopusnik, J. Mistrik, S. Stavroyiannis, and S. Visnovsky, Proceedings of the 3rd International Symposium on Metallic Multilayers (MML'98, Vancouver, Canada, June 1998), J. Magn. Magn. Mater. (to be published).
[34] A. Fuß, S. Demokritov, P. Grunberg, and W. Zinn, J. Magn. Magn. Mater. **103**, L221 (1992).
[35] J. C. Slonszewski, Phys. Rev. Lett. **67**, 3172 (1991).
[36] T. R. McGuire and R. I. Potter, IEEE Trans. Magn. **MAG-11**, 1018 (1975).
[37] S. Honda, T. Fujimoto, and M. Nawate, J. Appl. Phys. **80**, 5175 (1996).
[38] C. H. Lee, Hui He, F. J. Lamelas, W. Vavra, C. Uher, and R. Clarke, Phys. Rev. B **42**, 1066 (1990).
[39] H. P. Oepen, Y. T. Millev, and J. Kirchner, J. Appl. Phys. **81**, 5044 (1997).
[40] M. Sundaram, S. A. Chalmers, P. F. Hopkins, and A. C. Gossard, Science **254**, 1326 (1991).
[41] D. D. Champliss, R. J. Wilson, and S. Chiang, Phys. Rev. Lett. **66**, 1721 (1991).